

The relative importance of aeolian, sedimentary, and hydrothermal iron for supporting export production: estimates from an inverse model of the ocean's coupled phosphorus, silicon, and iron cycles

Benoît Pasquier^{1,2} and Mark Holzer²¹Department of Applied Mathematics, School of Mathematics and Statistics, University of New South Wales, Sydney, NSW, Australia.²Now at Department of Earth System Science, University of California, Irvine, CA, USA (email: pasquieb@uci.edu).

Introduction

The ocean's nutrient cycles control global primary productivity and the ocean's biological carbon pump. The cycles of macro and micronutrients are coupled through colimitation on biological uptake and through the scavenging of micronutrients by sinking organic matter. Dissolved iron (dFe) is a key micronutrient because of its fundamental role in limiting primary production.

We formulate an inverse model of the ocean's coupled P, Si, and Fe cycles embedded in a data-assimilated global circulation. The biogeochemical parameters are optimized to minimize the mismatch with observations. We improve on the Fe-cycle inverse model of [3] and produce, for the first time, a family of data-constrained state estimates of the coupled Fe–P–Si cycles for a wide range of aeolian, hydrothermal, and sedimentary sources.

We address an important open question about the Fe cycle: What are the relative efficiencies of the different iron sources in supporting the world ocean's export production? In addition to presenting the first inverse model of the coupled Fe–P–Si cycles, we address the following key scientific questions:

- How well can the modelled dFe, PO₄, and Si(OH)₄ concentrations be fitted to observations for widely differing iron sources?
- How well constrained are the P and Si exports for widely different iron sources?
- What fractions of the P and Si exports are supported by the different iron sources, and how do these fractions vary with the iron-source strengths?

1. Model

The steady-state tracer equations for the concentrations of PO₄, Si(OH)₄, and dFe (denoted by χ_P , χ_{Si} , and χ_{Fe}) are

$$\mathcal{T}\chi_P = \sum_c (S_c^P - 1)U_c - \gamma_g(\chi_P - \bar{\chi}_P^{obs}), \quad (1)$$

$$\mathcal{T}\chi_{Si} = (S^{Si} - 1)R^{Si:P}U_{dia} - \gamma_g(\chi_{Si} - \bar{\chi}_{Si}^{obs}), \quad (2)$$

$$\mathcal{T}\chi_{Fe} = \sum_c (S_c^{Fe} - 1)R^{Fe:P}U_c + (S^{POP} - 1)J_{POP} + (S^{bSi} - 1)J_{bSi} - J_{dst} + S_A + S_S + S_H. \quad (3)$$

\mathcal{T} is the advection-diffusion operator (transport matrix of [9]). U_c is the P-uptake rate per unit volume by phytoplankton functional class c . We model 3 classes: non-diatom small ($< 2 \mu\text{m}$, $c = \text{sml}$), non-diatom large ($\geq 2 \mu\text{m}$, $c = \text{lg}$), and diatoms ($c = \text{dia}$). $U_c \neq 0$ only in the model's euphotic zone, i.e., above 73.4 m (2 model layers). $R^{Si:P}$ and $R^{Fe:P}$ are the stoichiometric uptake ratios. S_c^P , S_c^{Si} , and S_c^{Fe} model the biogenic transport and remineralization by class c . J_{POP} , J_{bSi} , and J_{dst} are the scavenging rates by POP, opal particles (bSi), and mineral dust. S^{POP} and S^{bSi} model the particle transport of scavenged iron and its partial redissolution at depth. S_A , S_S , and S_H are the aeolian, sedimentary, and hydrothermal iron sources. We solve (1)–(3) using a fast Newton solver.

The uptake rates are a function of temperature T , irradiance I , and nutrient concentrations, and are calculated from phytoplankton concentration, ρ_c , and specific growth rate, μ_c , as

$$U_c = \mu_c \rho_c = \frac{\rho_c^{\max}}{\tau_c} e^{kT} (F_{I,c} F_{N,c})^2, \quad (4)$$

where τ_c is the timescale for growth, ρ_c^{\max} is the phytoplankton concentration under ideal conditions, and $F_{I,c}$ and $F_{N,c} \in [0, 1]$ represent light and nutrient limitation [2, 4].

The limitation of functional class c by nutrient i is a product of Monod factors:

$$F_{N,c} = \prod_i \frac{\chi_i}{\chi_i + k_c^i}. \quad (5)$$

The Fe:P uptake ratio is a simple Monod term as in [4]:

$$R^{Fe:P} = R_0^{Fe:P} \frac{\chi_{Fe}}{\chi_{Fe} + k_{Fe:P}}, \quad (6)$$

where $R_0^{Fe:P}$ is the maximal Fe:P uptake ratio. And the Si:P uptake ratio is modelled as

$$R^{Si:P} = R_0^{Si} + (R_m^{Si} - R_0^{Si}) \frac{k_{Si:P}^{Fe} \chi_{Si}}{\chi_{Fe} + k_{Si:P}^{Fe} \chi_{Si} + k_{Si:P}^{Si}}, \quad (7)$$

where the ratio involving χ_{Fe} produces increased silicification when iron is deficient, while the Monod term with χ_{Si} produces increased silicification in silicon-replete environments.

To produce a family of 287 objectively-optimized state estimates, we first set a number of unconstrainable parameters using literature values. We then optimize the remineralization profile using simple submodels. We finally optimize the constrainable parameters using the full coupled model. Because there is no scientific consensus on the Fe source strengths (which varies by 2 orders of magnitude), we then assign the Fe source strengths, and optimize the scavenging parameters and $R_0^{Fe:P}$. We finally re-optimize the Fe source strengths.

2. Results

The model–observation mismatches for P, Si, and Fe:

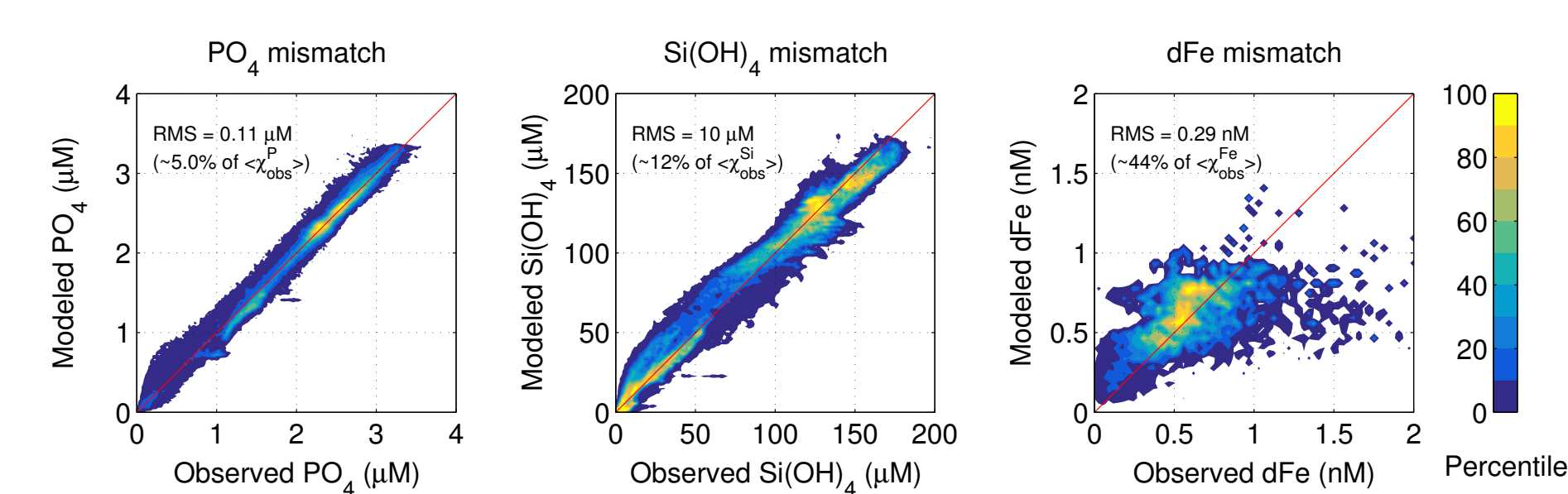


Figure 1: Joint distribution of the cost-weighted observed and modelled concentrations of PO₄, Si(OH)₄, and dFe. For PO₄ and Si(OH)₄, we used WOA13 observations. For dFe, we used the data compilation of [10] and the GEOTRACES IDP 2014 [7].

The cost function sums the volume-weighted mismatches, $E_i = \int (\chi_i - \chi_i^{obs})^2 dV$, for all state estimates:

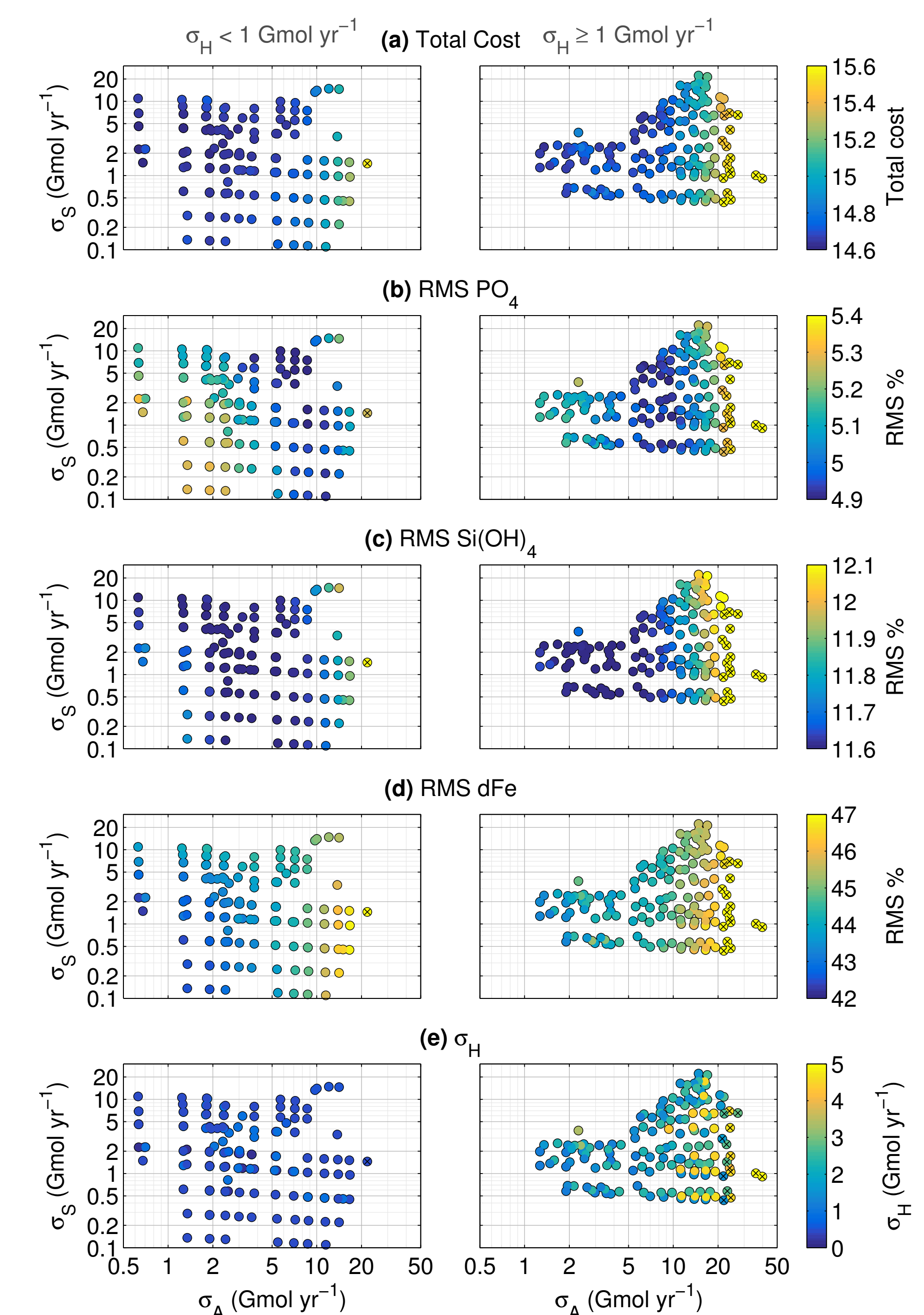


Figure 2: Total cost and RMS mismatch for the whole family of state estimates as a function of Fe sources (black crosses indicate outliers).

The modelled P, Si, and Fe exports, $\Phi^i = \sum_c \int_a dz S_c^i R_c^i U_c$:

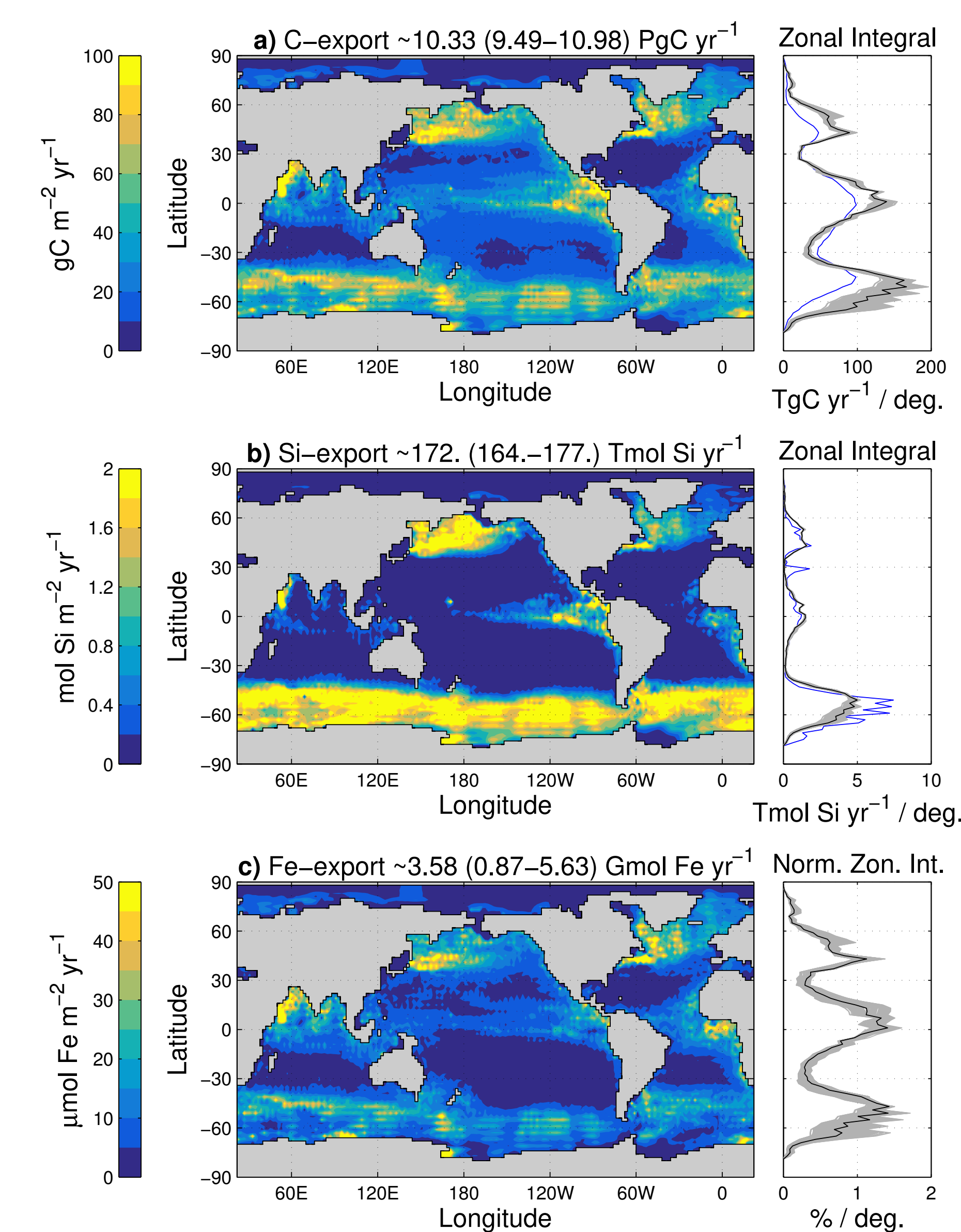


Figure 3: Local export production maps for our typical state estimate and zonal integrals (ZI, scaled for dFe) for whole family (grey) and typical state (black). (a) P export in C units using C:P = 106 : 1 (blue ZI from [9]). (b) Si export (blue ZI from [6]). (c) Iron export, with its zonal integrals expressed as a percentage of the global iron export. Global exports (typical estimate and family range) are indicated in each title.

The dFe partition according to source, $\chi_{Fe} = \chi_{Fe}^A + \chi_{Fe}^S + \chi_{Fe}^H$ [5]:

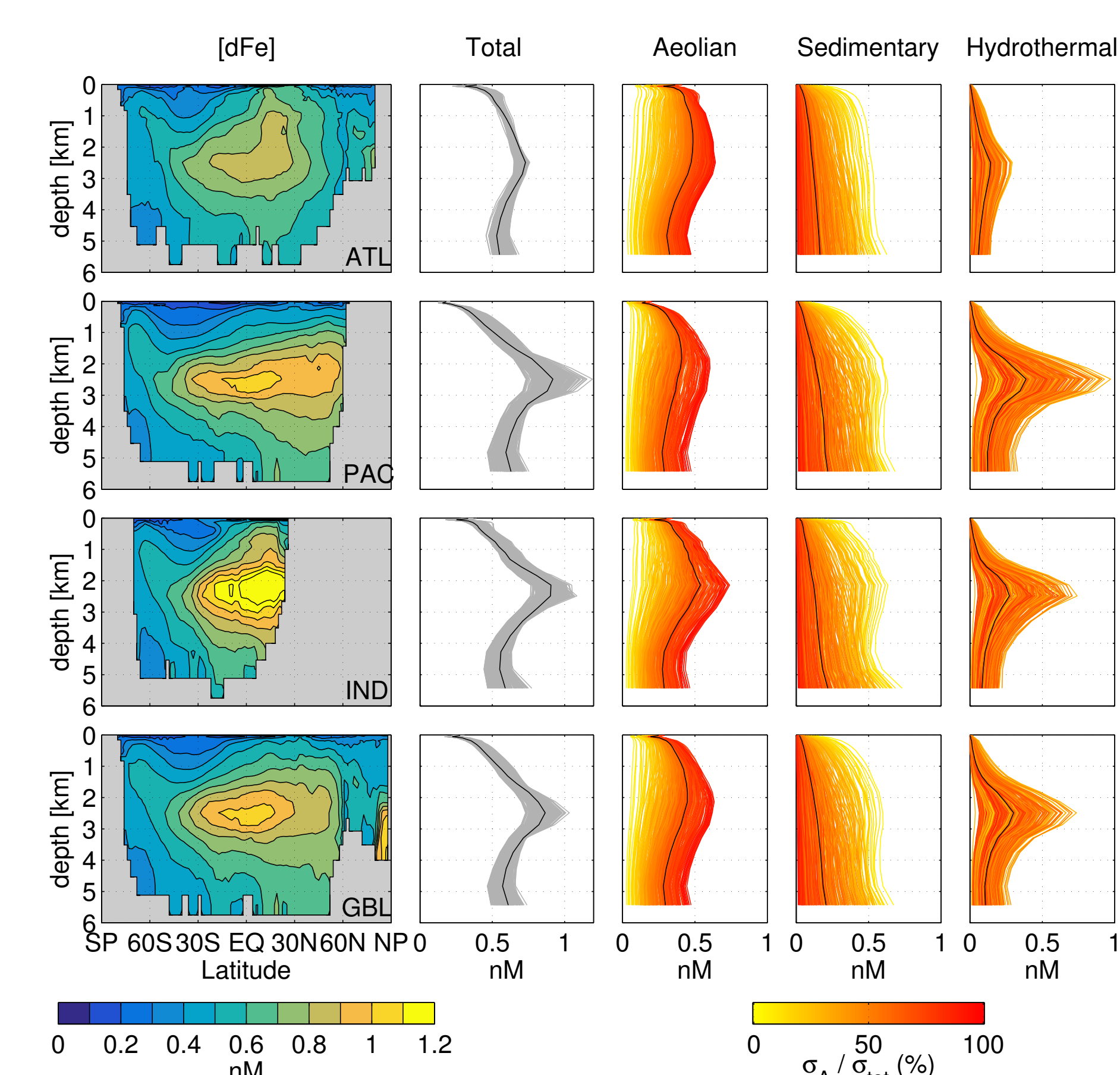


Figure 4: Estimates of the dFe concentration in each basin and globally (GBL). Left: zonal averages of total dFe for the typical state and corresponding horizontal averaged profiles (grey for the whole family and black for the typical state). Right: source-partitioned dFe profiles for each state (colour = fractional aeolian source and black = typical state).

The iron-type-supported P exports, $\Phi_k^P = \sum_c \int_a dz S_c^P U_c (\chi_k^c / \chi_{Fe}^c)$:

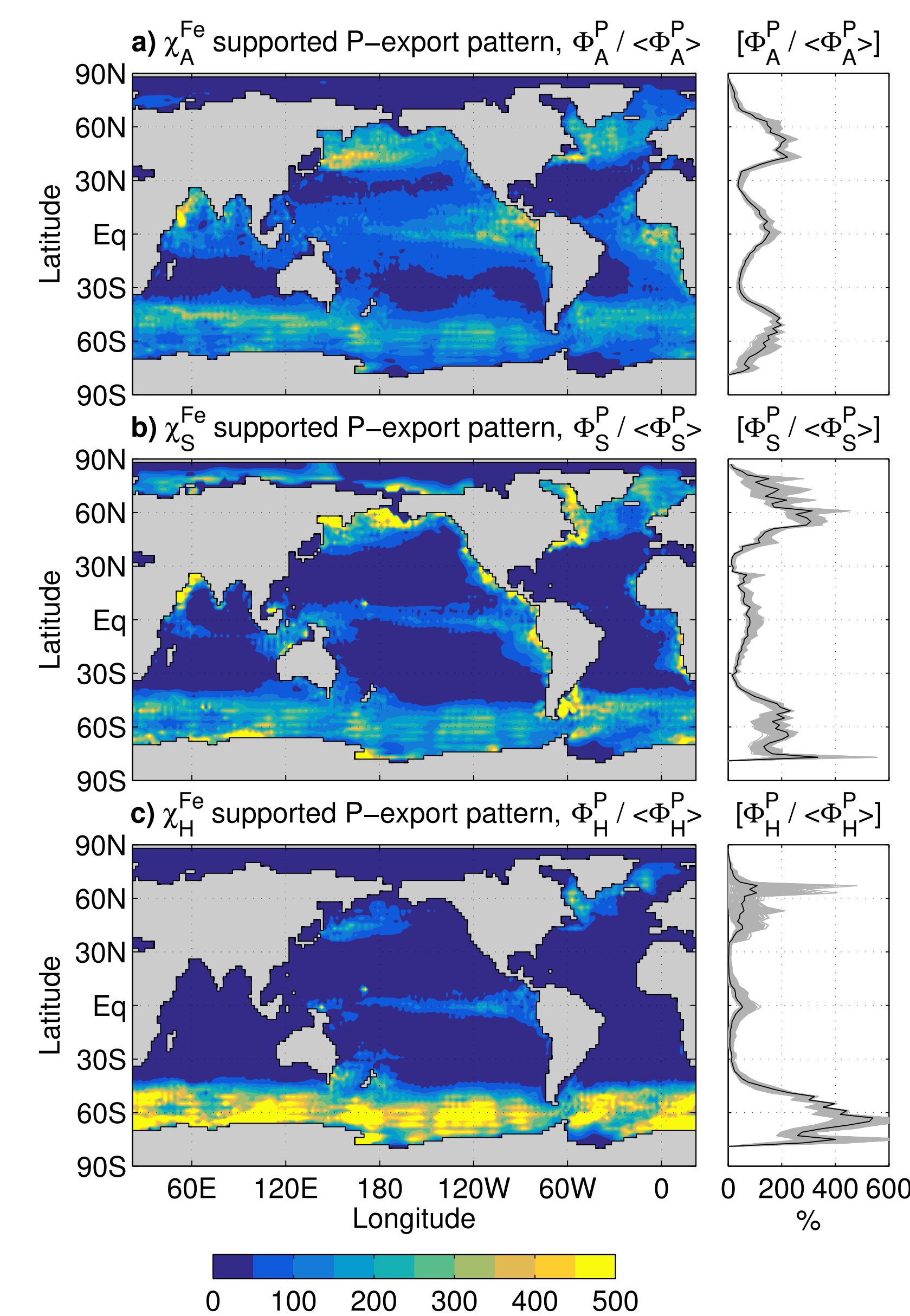


Figure 5: Maps of normalized P export supported by each iron type for the typical state and its zonal averages (grey is whole family and black is typical state).

The relative P export-support efficiencies, $e_k^P = \epsilon_k^P / \bar{\epsilon}_k^P$, where $\epsilon_k^P \equiv \hat{\Phi}_k^P / \hat{\sigma}_k$ and $\bar{\epsilon}_k^P = (1 - \hat{\Phi}_k^P) / (1 - \hat{\sigma}_k)$:

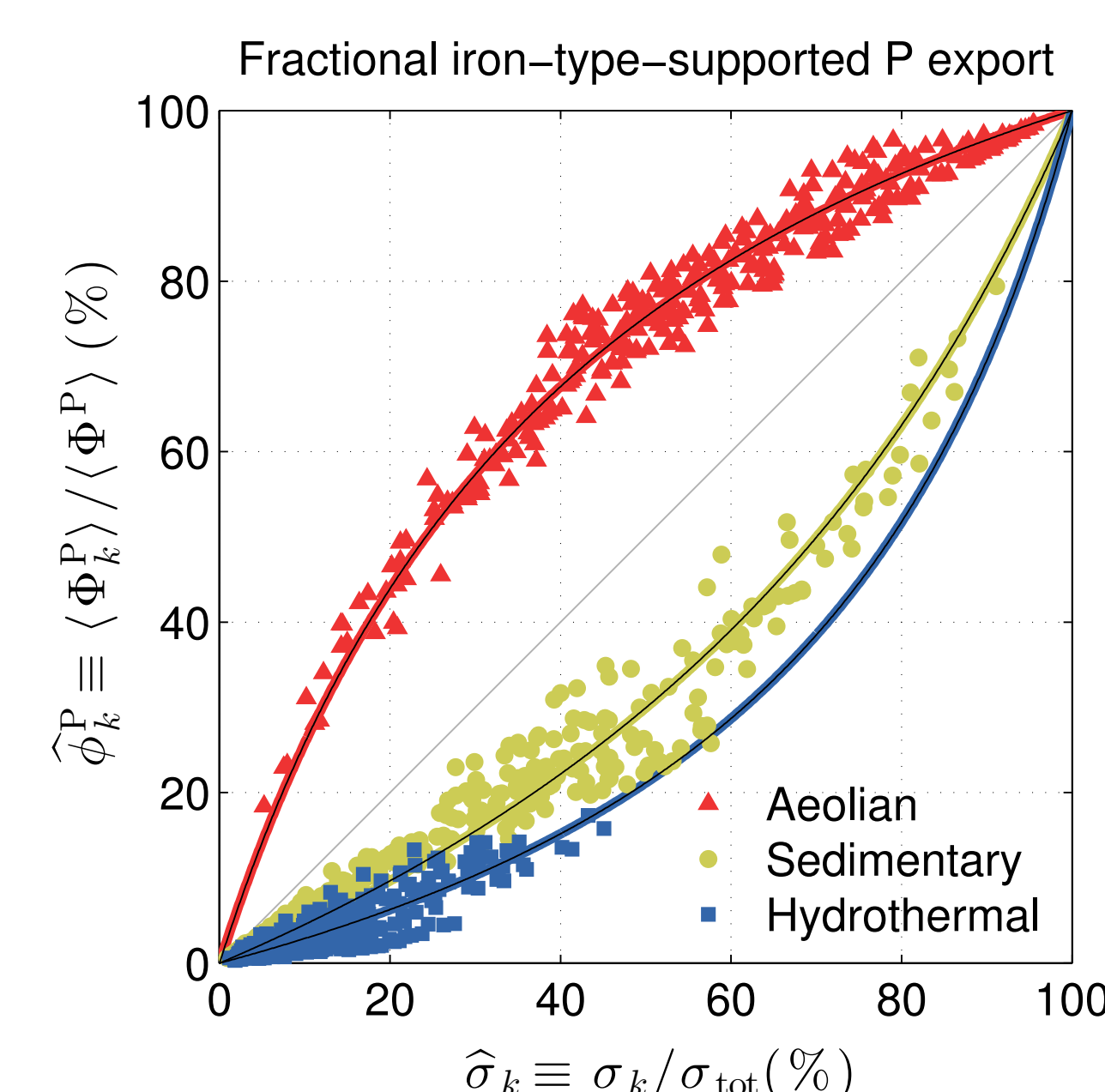


Figure 6: Percent global P export supported by each iron type vs the corresponding fractional source. Superposed lines are least-squares fits to the theoretical relationship with fixed relative export-support efficiencies, e_k^P .

3. Conclusions

- The relative simplicity of the biogeochemical model and the matrix formulation afford highly efficient numerics. Steady-state solutions are readily found using a Newton solver, which permits objective optimization of the biogeochemical parameters to minimize the mismatch with the observations.
- Our estimates of the PO₄ and Si(OH)₄ concentrations closely match the WOA13 observations with volume-weighted RMS errors of 5% and 12% relative to the global mean (Fig. 1). dFe has a larger RMS mismatch of $\sim 45\%$ relative to the global mean but the vertical dFe profiles for the Atlantic and Southern Ocean generally lie within the observational uncertainties (not shown, see [8]).
- We produced a family of state estimates with a wide range of Fe source strengths. Each estimate fits the observations with roughly the same fidelity (Fig. 2) because Fe sources are compensated by optimally adjusted scavenging: The available observed dFe are insufficient to constrain the sources.
- The P and Si exports are well constrained, both in pattern and magnitude (Fig. 3). Our P export estimates (in C units) of 9.5–11. Pg C yr⁻¹ is $\sim 40\%$ larger than [9] and closer in spatial pattern to the satellite-based estimates of [1]. The Si export of 164–177. Tmol Si yr⁻¹ overlaps with the estimates of [6].
- We partitioned dFe into its aeolian, sedimentary, and hydrothermal components without perturbing the system [5]. Variations in the one source are compensated by another despite their different geographical patterns (Fig. 4). Iron source–sink and source–source compensations suggest that more dFe observations may not allow to constrain the Fe sources, and that better direct quantification of the source and scavenging processes themselves are needed.
- Each iron source supports P and Si exports with a distinct geographic pattern (robust across the family, Fig. 5). Per source-injected molecule, aeolian iron is most efficient, while sedimentary and hydrothermal iron are less efficient, because dFe from deeper sources is more likely to be scavenged en route to the euphotic zone (Fig. 6). The relative export-support efficiency of each iron type is robust across our family of state estimates. Aeolian iron supports 3.1 ± 0.8 times more P export and 2.3 ± 0.5 times more Si export than the other iron types. Sedimentary and hydrothermal iron are respectively 2.3 ± 0.6 and $4. \pm 2.$ times less efficient in supporting P export, and 1.9 ± 0.5 and $2. \pm 1.$ times less efficient in supporting Si export, than the other iron types.

Our optimized model is ideally suited for investigating the response of the global ocean ecosystem to a variety of biogeochemical perturbations. In the future, we will report on the model's response to perturbations in the iron supply and on a more comprehensive analysis of the detailed workings of the iron cycle.

For all the details of this work, see [8].

Acknowledgements

We thank François Primeau for the transport matrices, Natalie Mahowald for the aeolian Fe flux estimates, and Marina Frants for discussions. This work was supported by ARC grant DP120100674 (MH). BP gratefully acknowledges scholarship support from the Government of Monaco, the Scientific Centre of Monaco, the Frères Louis et Max Principale Foundation, and the Cuomo Foundation. Poster presentation supported by DOE grant DE-SC0016539 (BP).

References

- J. P. Dunne, J. L. Sarmiento, and A. Gnanadesikan. "A synthesis of global particle export from the surface ocean and cycling through the ocean interior and on the seafloor". In: *Global Biogeochem. Cycles* 21, CB4006 (2007). doi: 10.1029/2006GB002907.
- J. P. Dunne, R. A. Armstrong, A. Gnanadesikan, and J. L. Sarmiento. "Empirical and Mechanistic Models for the Particle Export Ratio". In: *Global Biogeochem. Cycles* 19.4 (Dec. 2005). doi: 10.1029/2004gb002390.
- M. Frants, M. Holzer, T. DeVries, and R. Matear. "Constraints on the Global Marine Iron Cycle from a Simple Inverse Model". In: *Journal of Geophysical Research: Biogeosciences* 121.1 (Jan. 2016), pp. 28–51. doi: 10.1002/2015jg003111.
- E. D. Galbraith, A. Gnanadesikan, J. P. Dunne, and M. R. Hiscock. "Regional Impacts of Iron-Light Colimitation in a Global Biogeochemical Model". In: *Biogeosciences* 7.3 (Mar. 2010), pp. 1043–1064. doi: 10.5194/bg-7-1043-2010.
- M. Holzer, M. Frants, and B. Pasquier. "The age of iron and iron source attribution in the ocean". In: *Global Biogeochem. Cycles* (2016). 2016GB005418. issn: 1944-9224. doi: 10.1002/2016GB005418.
- M. Holzer, F. W. Primeau, T. DeVries, and R. Matear. "The Southern Ocean silicon trap: Data-constrained estimates of regenerated silicic acid, trapping efficiencies, and global transport paths". In: *Journal of Geophysical Research: Oceans* 119.1 (2014), pp. 313–331. issn: 2169-9291. doi: 10.1002/2013JC009356.
- E. Mawji et al. "The GEOTRACES Intermediate Data Product 2014". In: *Marine Chemistry* 177, Part 1 (2015). Biogeochemistry of trace elements and their isotopes, pp. 1–8. issn: 0304-4203. doi: 10.1016/j.marchem.2015.04.005.
- B. Pasquier and M. Holzer. "Inverse-model estimates of the ocean's coupled phosphorus, silicon, and iron cycles". In: *Biogeosciences Discussions* 2017 (2017), pp. 1–52. doi: 10.5194/bg-2017-122. url: https://www.biogeosciences-discuss.net/bg-2017-122/.
- F. W. Primeau, M. Holzer, and T. DeVries. "Southern Ocean nutrient trapping and the efficiency of the biological pump". In: *J. Geophys. Res.* 118 (2013), pp. 2547–2564. doi: 10.1002/jgrc.20181.
- A. Tagliabue, T. Mshali, O. Aumont, A. R. Bowie, M. B. Klunder, A. N. Roychoudhury, and S. Swart. "A global compilation of dissolved iron measurements: focus on distributions and processes in the Southern Ocean". In: *Biogeosciences* 9.6 (2012), pp. 2333–2349. doi: 10.5194/bg-9-2333-2012.